Development of 3D culture scaffolds for directional neuronal growth using 2-photon lithography

Development of 3D culture scaffolds for directional neuronal growth using 2-photon lithography

Lokesh Agrawal [a], Menouer Saidani [b], Laurent Guillaud [a], Marco Terenzio [a],[*]

[a] *Molecular Neuroscience Unit, Okinawa Institute of Science and Technology Graduate University, Kunigami-gun, Okinawa 904-0412, Japan*
[b] *Nanofabrication Team, Engineering Section, Okinawa Institute of Science and Technology Graduate University, Kunigami-gun, Okinawa 904-0412, Japan*

ARTICLE INFO

ABSTRACT

Conventional applications of transplant technology, applied to severe traumatic injuries of the nervous system, have met limited success in the clinics due to the complexity of restoring function to the damaged tissue. Neural tissue engineering aims to deploy scaffolds mimicking the physiological properties of the extracellular matrix to facilitate the elongation of axons and the repair of damaged nerves. However, the fabrication of ideal scaffolds with precisely controlled thickness, texture, porosity, alignment, and with the required mechanical strength, features needed for effective clinical applications, remains technically challenging. We took advantage of state-of-the-art 2-photon photolithography to fabricate highly ordered and biocompatible 3D nanogrid structures to enhance neuronal directional growth. First, we characterized the physical and chemical properties and proved the biocompatibility of said scaffolds by successfully culturing primary sensory and motor neurons on their surface. Interestingly, axons extended along the fibers with a high degree of alignment to the pattern of the nanogrid, as opposed to the lack of directionality observed on flat glass or polymeric surfaces, and could grow in 3D between different layers of the scaffold. The axonal growth pattern observed is highly desirable for the treatment of traumatic nerve damage occurring during peripheral and spinal cord injuries. Thus, our findings provide a proof of concept and explore the possibility of deploying aligned fibrous 3D scaffold/implants for the directed growth of axons, and could be used in the design of scaffolds targeted towards the restoration and repair of lost neuronal connections.

1. Introduction

Every year several million people worldwide suffer from spinal cord injury (SCI) [1], 15–40% of the cases also involving peripheral nerve injury (PNI) [2]. Over the last decade, regenerative medicine has achieved rapid and promising advancements in neural tissue engineering and stem cell therapy [3,4]. Neural tissue engineering (NTE) aims to improve regeneration of damaged nerves after injury and subsequent restoration of neuronal function using synthetic scaffolds, whose properties are fine tuned to mimic the extracellular matrix (ECM) [5–7]. The interaction between cells and ECM is critical, as the ECM provides cells with mechanical support and chemical cues for migration, differentiation, attachment, and morphological development [7–9]. Engineered scaffolds aim to achieve a structural framework that resembles the arrangement and function of the fibrous protein components of the ECM. Indeed, lesions bigger than 5 mm benefit from the use of artificial grafts to boost recovery and re-growth of the residual cells. In addition, physical, chemical and electrical cues have been tested alone or in combination to promote regeneration of damaged tissues. Physical cues to improve re-growth have been widely explored and a wide array of materials has been tested for their structural and chemical properties. Natural polymers, synthetic polymers and composites of both have been used for the fabrication of scaffolds [10,11]. Natural polymers provide relevant bionics properties and cell signaling cues but offer little control over scaffold structural or architectural properties (*i.e.*, fiber diameter, alignment, or porosity) [12,13]. Conversely, synthetic polymers provide fine control over the scaffold micro-architecture, but lack biocompatibility, thus requiring additional engineering [12]. Scaffolds can be

classified into two major categories, randomly oriented and aligned, based on their structural alignment [10]. The aim of an ideal aligned fiber scaffold is to create a mechanical framework to support neuronal adhesion and growth by recreating the structural features of their native fibrous substrates combined with the protein motifs present in the ECM [9,14–16]. Indeed, scaffolds made of aligned nanofibers favor neural stem cell attachment and proliferation, with clear benefits for the treatment of nerve injury [17]. Potential applications of aligned scaffolds are not limited to neuronal growth, as aligned arrays of fibers enhance orientation and cell migration and play an important role in a wide variety of biological processes including embryogenesis, wound healing, inflammation, and tissue repair [9,14,18].

Single layered aligned fiber scaffolds with limited thickness can be fabricated using a rotating disc or mandrel, patterned electrodes, air-gap techniques, a patterned insulator, or high strength ceramic or electromagnets with copper plates [10,17,19–22]. Such structures are ideal for the regeneration of monolayer tissues, such as skin, small vessel, tendons and ligaments [23–25]. Applications targeted to relatively large areas, like treatment of myocardial infarction, spinal cord injury, nerve injury, cartilage and bone necrosis, and tumor removal, require scaffolds with a substantial thickness and precisely controlled architecture [23,24]. Design and fabrication of such scaffolds with highly aligned fibers, a precisely controlled morphology and textures suitable for surgical applications is, however, challenging under current technological limitations. Indeed, most fabrication techniques do not allow for the precise control of the aforementioned parameters. Interestingly, two-photon polymerization (2-PP) laser lithography has emerged in recent years as a powerful technology to fabricate custom scaffolds to accommodate the needs of specific cell types and recapitulate *in vivo* biomimetic cues [26]. Indeed, 2-PP has been used to produce porous devices with varied dimensions and the geometry designed to positively impact cell proliferation, differentiation and migration [27–29]. Further, photo-resins have been utilized to fabricate sub-micrometric patterns to direct the growth of neurons and promote the formation of neuronal networks [30].

In light of the aforementioned studies, we took advantage of 2-PP laser lithography to generate nanopatterns of few hundred nanometers resolution and high mechanical strength, using IP-Dip photoresist, a commercially available liquid negative-tone resin, which allows for the high resolution printing of 3D scaffolds with defined features, enabling us to finely control the porosity and texture of our structures to mimic ECM architecture and to improve steering the growth of axons. We then characterized the physical and chemical properties of IP-Dip polymeric surfaces and fibers. In addition, we tested scaffold biocompatibility for sensory dorsal ganglia (DRG) and motor (MNs) neurons, which are relevant neuronal types for the treatment of peripheral (PNI) and spinal cord injuries (SCI). Tests included validation of neuronal ability for vectorized axonal growth and generation of an orchestrated 3D axonal network inside the scaffold. Our *ex vivo* results provide a proof of concept that orchestrated nanofibers promote both 3D and vectorized growth of axons inside the scaffold and along the length of the fibers and set a basis for the design of implants for the promotion of nerve regeneration *in vivo*.

2. Materials and methods

2.1. Ethics statement

All experiments were carried out following the guidelines of the Okinawa Institute of Science and Technology Graduate University (OIST) genetic manipulation procedures. All animal experiments have been performed in accordance to the regulations of OIST animal care and use committee. OIST animal facilities and animal care and use program are accredited by AAALAC International (Ref. #1551).

2.2. Chemicals and reagents

All chemicals were supplied by Sigma Aldrich, unless stated otherwise. Photoresist IP-Dip (Nanoscribe GMBH, Germany) was used for the lithography of the 3D scaffold. SYLGARD™ 184 silicon elastomer kit (Dow, USA) was used to prepare cured PDMS ring for the culture chamber. Propylene glycol methyl ether acetate (PGMEA) and Isopropyl Alcohol (IPA) were purchased from Sigma Aldrich. Suppliers for tissue culture media and supplements are individually specified in the method section. Anti-βIII tubulin antibody was purchased from GeneTex (#GTX631830) and Alexa AlexaFlour 568 anti-mouse secondary antibody was purchased from ThermoFisher Scientific, Japan.

2.3. Design and fabrication of IP-Dip nanofiber grids

Nanofiber grids were designed using CAD-software Rhino 3D (Robert McNeel & Associates, U.S.A.). A mesh was generated and exported as a STL file for 3D lithography. STL files were imported into the DeScribe software (Nanoscribe GmbH, Germany), which displays a 3D preview of the model and sets writing parameters, such as rescaling, structure's slicing and planes filling lines, which represent the laser scanning paths. The 3D model (along with all the writing parameters) was then transferred into the NanoWrite printing interface, which executes the print job. A 25 mm × 25 mm ITO-coated (ITO improves interface finding between the photoresist and the glass surface) fused silica substrate was cleaned using an Acetone/IPA/water sonication cycle, followed by 30 min dehydration at 150 °C. The substrate was then attached to the Nanoscribe Photonic Professional GT 3D printer holder and a drop of IP-Dip photoresist (Nanoscribe GmbH, Germany) was applied. The substrate holder was then mounted on the Nanoscribe stage together with a 63× objective (Carl Zeiss AG, Germany) for high resolution printing. The structure was printed by scanning the laser following the model's slicing/filling path lines. The stage movement is a combination of Galvo-X/Y- and Piezo-Z stages to reproduce the 3D model rapidly and precisely. The IP-Dip photoresist was exposed to a 100-fs laser at 780 nm wavelength. Once the nano-3D-printing was completed, the substrate was removed and developed in Propylene glycol methyl ether acetate (PGMEA, Sigma-Aldrich, #484431). The structure was subsequently rinsed in IPA (Sigma-Aldrich, #W292907) and dried, to obtain the final free-standing nanofiber 3D scaffold.

2.4. Physio-chemical characterization

2.4.1. Thermal properties analysis

A DSC 8500 (PerkinElmer) was used for the thermal analysis of the IP-Dip nanogrid scaffold. Photoresist sample of 25 mg were placed in alumina pans and empty pans were used as a reference. All samples were first heated at a range of 40 to 250 °C at a heating rate of 10 °C/min. Afterwards, the samples were cooled to 40 °C at 10 °C/min. After each test, the melting point region from the thermograph was analyzed to determine the melting temperature (Tm).

2.4.2. Atomic force microscopy (ATM)-based mechanical analysis

AFM images of the nanogrid were acquired using a MultiMode 8 Atomic Force Microscope with a Nanoscope V controller and E scanner (Bruker). Mechanical studies of scaffold nanofibers were performed using a PeakForceTapping mode. AFM imaging was conducted with RTESPA-300 probe (Bruker) with a nominal spring constant of 5.1 N/m, nominal frequency of 2 kHz and a nominal tip radius of 15 nm [31]. Nanogrid scaffolds were studied in air over the area of 50×50 μm^2 and 5×5 μm^2 to determine force-displacement curves. The reduced Young's Modulus/DMT modulus, is calculated by the software by fitting the retract curve using the Derjaguin, Muller, Toropov (DMT) model [32]. Images were obtained at a scan rate of 1 Hz and 512×512 pixels' resolution. The raw Young's modulus AFM images were processed using the NanoScope Analysis v.1.10 software (Bruker).

2.4.3. Contact angle measurement

The wettability of the photolithographed IP-Dip surfaces was evaluated by static contact angle measurement using an Easy Drop tensiometer (KRUSS, GmbH). The contact angle is a quantitative measure of the wetting of a solid by liquid and is dependent on the surface area, with higher surface energies being associated with lower contact angles [33]. A water droplet was poured on the surface of solid samples and the contact angle was measured by Drop Shape Analysis (DSA) software (KRUSS, GmbH).

2.4.4. Development of an in-house culture chamber

For the fabrication of Polydimethylsiloxane (PDMS) rings, molds were designed using Rhino software and 3D printed using Stratasys Objet500 Connex3 multi-material 3D printer (Stratasys Ltd., U.S.A.). PDMS pre-polymer and catalyst were then mixed thoroughly with a 10:1 ratio in a disposable plastic cup. The mixture was degassed in a vacuum desiccator for 20 min and poured inside the molds. The PDMS was cured in an oven at 60 °C for 3 h. Finally, polymerized PDMS rings were extracted from the molds and fixed on the glass slide keeping the laser-printed nanogrid at the center of the ring to create a chamber for neuronal culture. To bond the rings onto the glass surface, PDMS polymeric solution was applied as a glue at the bottom of the ring and cured for 4 h. Before culture, the PDMS rings bonded to glass were sterilized and tested for possible leaks by filling with 99.99% ethanol for 5 min followed by sterile water for 15 min.

2.4.5. Quantification of the IP-Dip scaffold auto-fluorescence (AF)

The software ImageJ (National Institute of Health, U.S.A.; http://imagej.nih.gov/ij/) was used to measure the integrated density (ID) and mean gray values of the scaffold from the confocal images. The following formula (1) was used to quantify the AF from the nanogrid at different wavelengths (Luke Hammond, QBI, University of Queensland; https://theolb.readthedocs.io/en/latest/imaging/measuring-cell-fluorescence-using-imagej.html#).

$$AF = ID - (\text{Area of the selected pixels} \times \text{Mean fluorescence of background})$$
(1)

2.5. Ex vivo culture of dorsal root ganglia (DRG) and embryonic motor neurons

2.5.1. Culture of dorsal root ganglia (DRG) neurons

The IP-Dip scaffold was sterilized with 99.99% EtOH for 5 min. The alcohol was left to evaporate and rinsed with water. The structure was then coated with 0.01% Poly-L-lysine (Sigma-Aldrich # P4832-50 ml) overnight at 4 °C, rinsed with water and coated again with laminin (GibcoBRL #23017-015) for 2 h at 4 °C. DRGs were dissected from 2 months old ICR mice (Charles River or JapanClea, Japan) and dissociated as previously described by Ben-Yaakov et al. [34]. Briefly, after dissection, DRGs were dissociated by serial digestion with 100 U of papain (Sigma-Aldrich, #P4762) in HBSS (GibcoBRL, #14175095), followed by digestion with 1 mg/ml collagenase-II (Worthington Biochemical Corporation, #CLS2) and 1.2 mg/ml dispase (Roche Diagnostics GmbH, #04942078001) at 37 °C in HBSS for at least 30 min. The ganglia were then triturated in HBSS, 10 mM Glucose, and 5 mM HEPES (Sigma-Aldrich, #H0887), pH 7.35. Cells were recovered by centrifugation through 20% Percoll (Sigma-Aldrich, #P4937) in L15 medium (GibcoBRL, #L-5520) at the speed of 1000 rpm for 7 min, plated at a density of 2×10^4 cells/scaffold and grown in F12 medium (GibcoBRL, #11765054) for 48 h.

2.5.2. Culture of embryonic motor neurons

C57/BL6 mouse embryonic stem cells (mESC, #SCRC-1002, ATCC, USA) were cultured and maintained as previously described [35]. Briefly, mESCs were maintained on gelatin coated flasks (EmbryoMax

0.1% Gelatin solution, Merck, #ES-006-B) in Glasgow Minimal Essential Medium (GMEM, GibcoBRL #11710035), 5% ES cell-qualified fetal bovine serum (FBS, GibcoBRL, #16141079), 5% knockout serum replacement (KSR, GibcoBRL, #10828028), 1% GlutaMAX (GibcoBRL, #35050061), 0.1 mM 2-mercaptoethanol and 1000 units/ml of leukemia inhibitory factor (Chemicon International, Inc., #ESG1107). Motor neurons were generated by growing 1.5×10^6 mESC in suspension on a 10 cm non-tissue culture treated Petri dish in presence of differentiation medium (DFNK): 45% Neurobasal (GibcoBRL, #21103049), 45% DMEM/Ham's-F12 (FUJIFILM Wako #041-29775/ GibcoBRL #11765062), 10% KSR, 1% GlutaMAX and 0.1 mM 2-mercaptoethanol. The day after plating, embryoid bodies (EBs) were gently centrifuged and re-suspended in 10 ml of DFNK medium in a new Petri dish. 24 h later, EBs were allowed to sediment by gravity and re-suspended in fresh DFNK medium supplemented with 1 μM all-trans retinoic acid (RA, Sigma-Aldrich, #R2625) and 333 nM Smoothened Agonist (SAG; Merck, #566660) and maintained as such for additional 4 days (the medium was changed every other day). Finally, EBs were dissociated with trypsin-EDTA (Sigma-Aldrich, #T4049) for 7 min at 37 °C as previously described [36]. The IP-Dip scaffold was sterilized with 99.99% EtOH for 5 min, left to evaporate and rinsed with water. The structure was then coated with 0.01% Poly-L-lysine overnight at 4 °C, rinsed with water and coated again with laminin for 2 h at 4 °C. Dissociated motor neurons were plated onto the scaffold in motor neuron growth medium: Neurobasal medium (GibcoBRL, #21103049) supplemented with 2% B27 (ThermoFisher, #12587010), 2% FBS, 1% GlutaMAX, 25 μM 2-mercaptoethanol, 10 ng/ml rat ciliary neurotrophic factor (CNTF; Peprotech, #450–13), 100 pg/ml rat glial cell line-derived neurotrophic factor (GDNF; Peprotech, #450-10) and 1 μM RA.

2.5.3. Cell viability assay

Survival analysis of DRG neurons grown on IP-Dip polymeric surfaces was performed to assess the biocompatibility of the material. A flat 3 mm × 3 mm × 10 μm (L × W × H) IP-Dip structure was printed by 2-PP lithography (Nanoscribe GMBH) (Fig. S3). DRG neurons were dissected and cultured as previously explained and cell viability was determined using the CytoPainter Fixable Cell Viability Assay Kit (Fluorometric–Red; ab176744) according to manufacturer's instructions. Briefly, 48 h after plating, the culture medium was replaced with HBSS buffer (300 μl) containing tracking red dye (1 μl). Cells were incubated at 37 °C for 45 min and washed with HBSS followed by fixation with 4% paraformaldehyde (Electron Microscopy Sciences, #15710) in phosphate buffer saline (PBS) for 30 min at room temperature. Fluorescence imaging was performed on a confocal laser scanning microscope LSM900 (Carl Zeiss AG, Germany) using 63× oil immersion objective (Plan-Apochromat DIC M27, NA = 1.40) and 561 nm excitation laser line. Tiling and 1 μm z-stacks images (512 × 512 pixels resolution) were scanned to encompass the entirety of the IP-Dip polymeric surfaces.

2.5.4. Scanning electron microscopy (SEM) imaging

We followed the protocol described in our previously published paper with some modifications [37]. Cultured DRG neurons were fixed with 2.5% glutaraldehyde for 20 min. After fixation, cells were washed 3 times with PBS (e-Nacalai, #14249-95) for 1 min. Samples were then fixed with 1% Osmium tetraoxide for 20 min, washed 5 times with PBS for 5 min each. Samples were then gradually dehydrated with 70%, 90%, and 100% EtOH for 15 min and then subjected to t-butyl alcohol (Sigma-Aldrich #471712), to freeze at −30 °C for 5 min. Frozen samples were kept inside the Freeze Dryer (ES-2030) at −20 °C under vacuum and dried overnight. Finally, dried samples were coated with gold using a multifunction vacuum sputter deposition equipment for 3 min at 0.001 Pa. SEM images were acquired with SEM (JEOL JSM-7900F) at a positive voltage of 5 kV current with LED detector at magnifications ranging from 850× to 8500×.
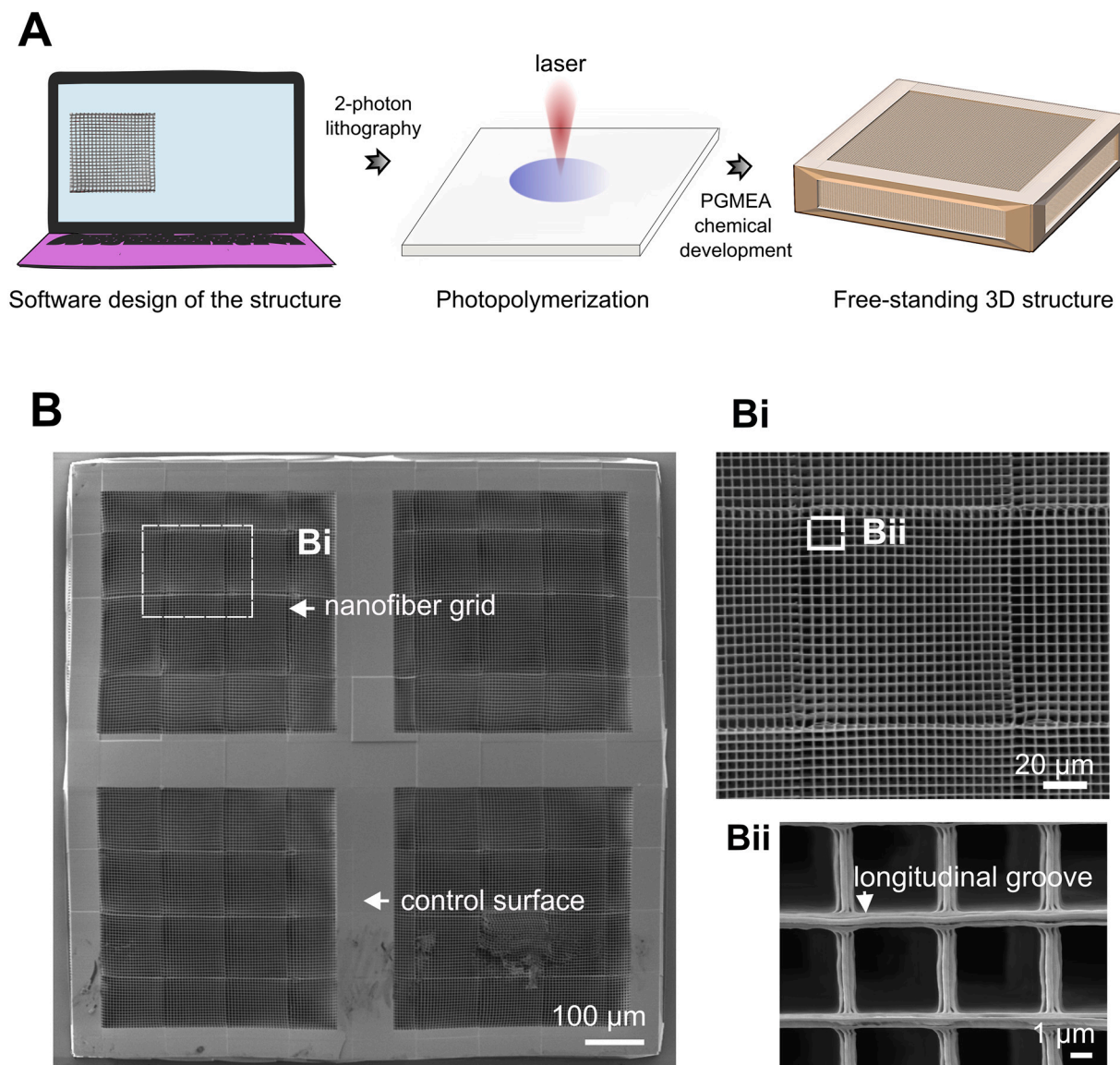
Fig. 1. Fabrication of IP-Dip nanogrid using two-photon lithography. (A) The 3D nanogrid was designed using computer aided design software. Next, photolithography was used to print the IP-Dip scaffold. Finally, the nanogrid was chemically developed. (B) SEM image of IP-Dip 3D scaffold. (Bi) magnified view of the aligned fiber mesh. (Bii) Ultrastructure of the surface morphology of single fibers, where the feature of longitudinal grooves is highlighted. Scale bars: 100 μm (B), 20 μm (Bi), 1 μm (Bii).

2.5.5. Immunohistochemistry

DRG neurons were cultured for 2 days and MNs for 4 day as described above and fixed with 4% paraformaldehyde (Electron Microscopy Sciences, #15710) in phosphate buffer saline (PBS) for 30 min at room temperature. Nonspecific antibody binding was blocked by incubation with 2% normal goat serum and 0.1% Triton X-100 in PBS for 30 min. To visualize the axonal network, neurons were incubated overnight at 4 °C with anti-βIII-tubulin antibody (1:1000 dilution in PBS). Cells were then washed 3 times with PBS and incubated with anti-mouse AlexaFluor 568 conjugated secondary antibody (1:500 dilution in PBS) for 1 h at room temperature. The AlexaFluor 568 fluorophore was chosen after assessing the auto-fluorescence properties of the nanogrid scaffold. Fluorescence imaging was performed on a confocal laser scanning microscope LSM900 (Carl Zeiss AG, Germany) using 63× oil immersion objective (Plan-Apochromat DIC M27, NA = 1.40). Images were acquired in ZenBlue 3.1 (Carl Zeiss AG, Germany) with a 512 × 512 pixel resolution and a 2.05 μs pixel dwell time. A 3 × 3 tiles and z-stacks (with 1 μm steps) image was scanned to encompass the entire grid scaffold on xyz planes. After stitching tiles, the resulting image had a

Table 1
Physio-chemical characterization of IP-Dip 3D scaffolds. Summary of the measurements taken to characterize the physical and chemical properties of IP-Dip scaffolds. Fiber's diameter, water contact angle, scaffold's melting temperature and mechanical strength are reported as mean values $\pm$ standard error of the mean (s.e.m., $n = 3$) where appropriate.

Measurement	Numeric values
Morphological analysis: Fiber diameter	1 μm
Wettability measurement: Contact angle (in degrees)	$77.702 \pm 5.580°$
Thermal stability: Melting temperature	220.06 ± 2.441 °C
Mechanical strength: Young's modulus	594.35 ± 73.01 MPa

A

Bi **Bii**

C **D**
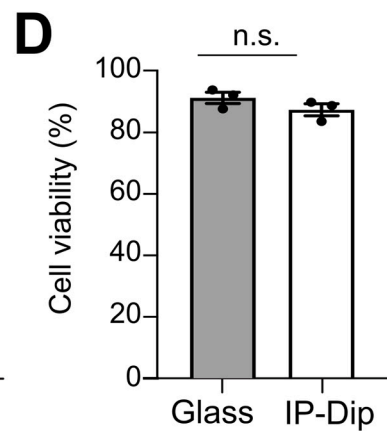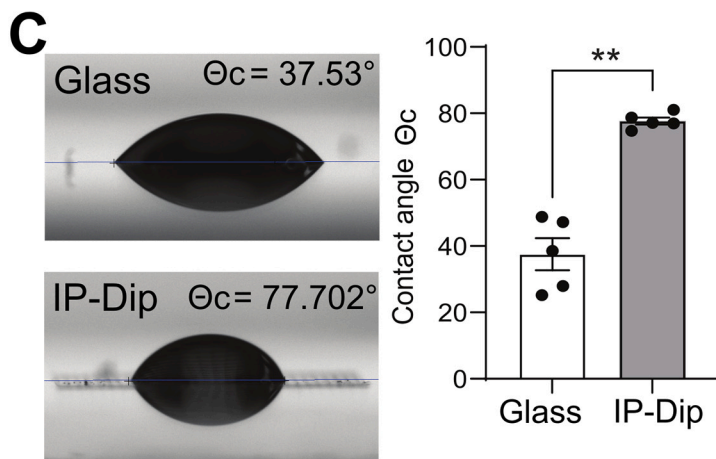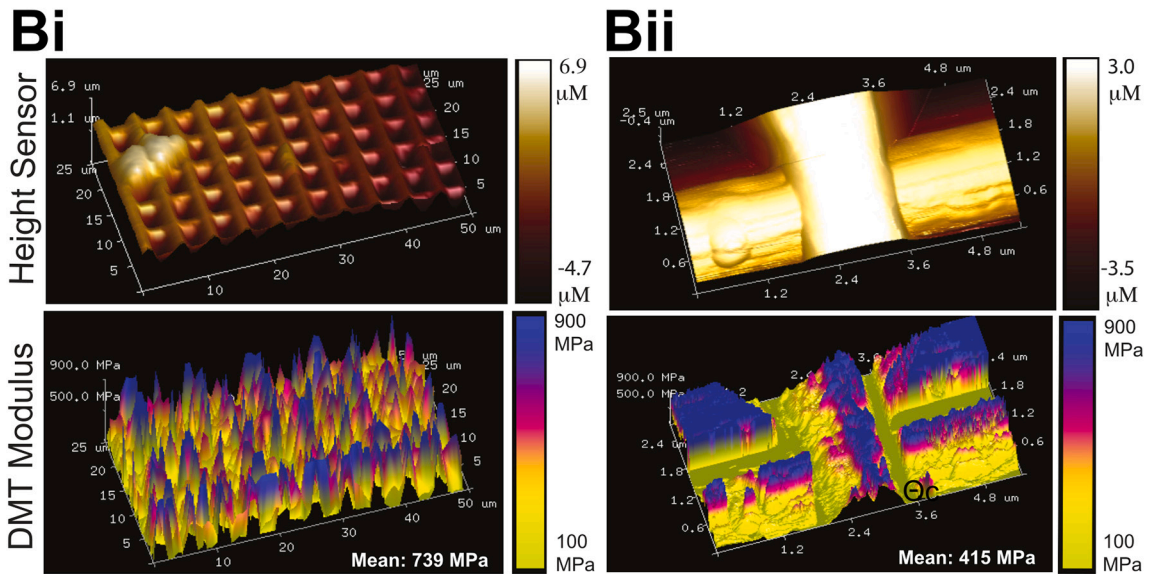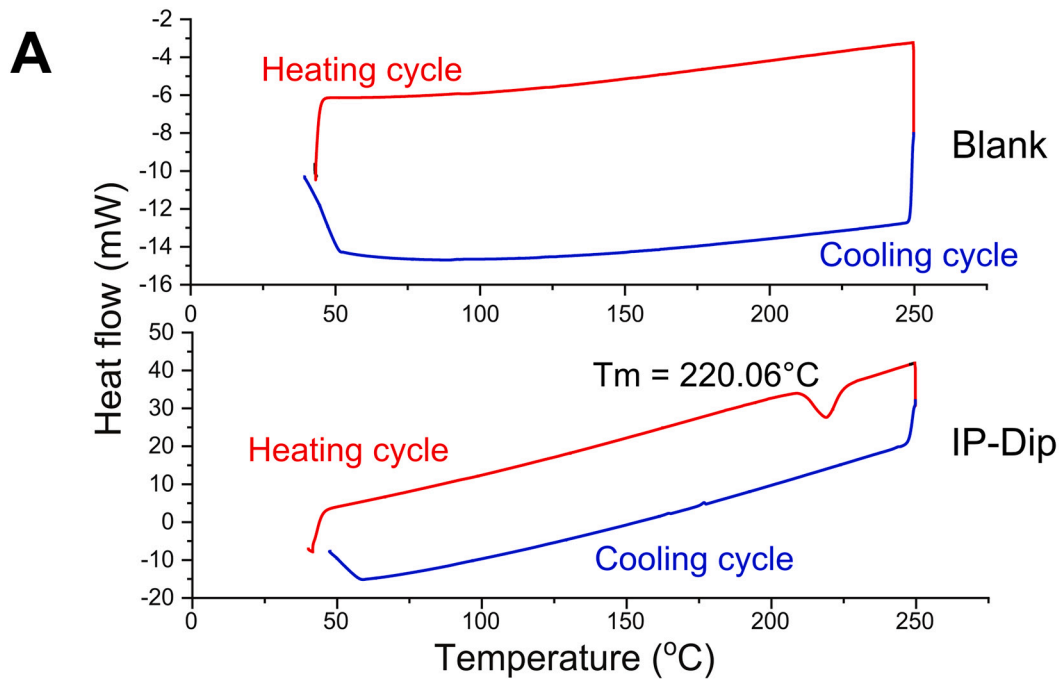
(caption on next page)

Fig. 2. Physio-chemical characterization of IP-Dip surfaces and scaffolds. (A) Differential scanning caliometry (DSC) curves of the IP-Dip surface showing a heating (in red) and cooling cycle (in blue). This curve illustrates the thermal behavior of the blank sample and IP-Dip photoresist. During heating cycle an endothermic melting peak occurs at 220.06 ± 2.441 °C. The data suggest that the polymer is highly stable at room temperature and thus a suitable candidate for being used as an implant or conduit in an *in vivo* setting. (B) Representative AFM images of an IP-Dip scaffold (Bi) and single fibers within it (Bii), showing the high sensor readings (high Sensor) and anisotropic distribution of the calculated Young's modulus (DMT modulus). (C) Representative images of a water drop on glass (control surface) and IP-Dip surfaces. On the side, quantification of the static water contact angle of glass and IP-Dip surface. Data are shown as mean ± s.e.m.; asterisks indicate statistical significance (Student *t*-test; **$p < 0.01$). (D) Quantification of the percentage of viable cells. No significant difference was found between the two materials (Student t-test). Data is shown as mean ± s.e.m. The total number of cells analyzed on the control glass surface and polymeric IP-Dip surface is 736 and 1291 respectively, over 3 biological independent replicates ($n = 3$). Scale bar: 500 μM (Bi) and 5 μM (Bii). (For interpretation of the references to color in this figure legend, the reader is referred to the web version of this article.)

final xy resolution of 1433 × 1434 pixels (1 pixel = 0.396 μm). Stitched images were either transferred to Imaris 9.5.1 (Bitplane AG/Oxford Instruments, UK) for 3D surface rendering or processed with maximum intensity projection filter (ZenBlue 3.1) and digitally zoomed by 8× for image analysis and quantification of axon orientation index (see below).

2.6. Quantification of neuronal orientation

Axonal orientation of neurons grown on glass, plain IP-Dip surface and aligned IP-Dip fibers, was determined to investigate the effects of the aligned fibers on neurite growth. Maximum intensity projection of confocal images of β3-tubulin stained DRG neurons were used for the neurite outgrowth analysis. Areas of 170 × 85 μm² (length × width) were analyzed. The OrientationJ plugin of the ImageJ software was used to quantitatively analyze the directionality of neurites. OrientationJ computes local orientations of each pixel, which are then encoded in colors (HSB color mapped by orientation angles of neurons) and displayed directly on the images (Fig. 4). Polar frequency histograms of local pixel distribution were then produced using OriginPro software (Origin Lab Corp., U.S.A.). The angular color scale in polar frequency histogram has been kept consistent with the color coding of the OrientationJ plugin.

Further, we calculated the orientation index (OI) for neurites growing parallel to the x-axis (0°) of the nanogrid (along the fibers), using the method described by Eunhee Kim and colleagues [26] using the following formula (2):

$$OI\ (\theta_i = 0°) = \frac{\sum_{\theta=-90°}^{90°} cos(2(\theta))N(\theta)}{\sum_{\theta=-90°}^{90°} N(\theta)} \quad (2)$$

θ_i is the alignment angle of interest (0° in our calculations), θ is the local orientation angle, and N(θ) is the frequency of pixels at a given orientation angle. The values of OI ranges from 1 (θ = 0°; cos 2θ = 1) to −1 (θ = 90° or −90°; cos 2θ = −1) depending on the orientation angle of the pixels. OI values of 1 and −1 indicate completely parallel and orthogonal alignments, respectively, relative to the x-axis. OI values closer to 0 indicate arbitrary isotropic directionality. The quantification of OI measurement was done in arbitrary units (a.u.). The normalized polar frequency (N_f) histograms were prepared and plotted against the orientation angles for the values from 90° to −90° using the following formula (3):

$$N_f(\theta) = N(\theta) \bigg/ \sum_{\theta=-90°}^{90°} N(\theta) \quad (3)$$

In order to determine the dominant orientation of the angles, the distribution of angles was categorized in 6 clusters: −90° to −60°, −60° to −30° and −30° to 0°, 0° to 30°, 30° to 60°, 60° to 90°. The average pixels frequency was calculated for each bin, normalized using the Eq. (3) and plotted against the angular range of the clusters.

2.7. Image processing

Maximum intensity projections of confocal Z stacks were created using ZenBlue 3.1 (Carl Zeiss AG, Germany). Imaris 9.5.1 (Bitplane AG/Oxford Instruments, UK) was used for the 3D surface rendering of

immunofluorescence images. Binary images and HSB color mapped images were prepared using ImageJ (National Institute of Health, U.S.A.; http://imagej.nih.gov/ij/). Inkscape: Open Source Scalable Vector Graphics Editor (https://inkscape.org/) was used for to prepare the final figures.

2.8. Statistical analysis

GraphPad Prism 9 Software, (GraphPad, U.S.A.) was used for the statistical analysis. ANOVA with Tukey's *post hoc* test was performed for multiple comparisons. Differences were considered significant if the probability of error was less than 5%. All the data were expressed as mean ± s.e.m., error bar indicates standard error of mean. *$p < 0.05$, **$p < 0.01$, ***$p < 0.001$, and ****$p < 0.0001$.

3. Results

3.1. Fabrication and structural characterization

Laser 2-PP photolithography allows for the generation of fine patterns with the resolution of few hundred nanometers and high mechanical strength, making the fabrication of high resolution 3D scaffolds with finely controlled porosity, alignment and texture possible [26]. Taking advantage of this technique, a 3D solid scaffold was produced within IP-Dip photoresist, a liquid negative-tone resin designed by Nanoscribe for printing of high resolution 3D features (Fig. 1A). The use of IP-Dip allowed us to achieve printing details on the fibers, such as indentations/funnels, up to a theoretical size of 200 nm. We designed a scaffold with an overall dimension of 1 mm × 1 mm × 100 μm (L × W × H) (Fig. 1B). Fiber diameter (1 μm) and inter-fiber spacing (5 μm) were chosen to accommodate the size of DRG and motor neurons somata and neurites, which range in the order of tens of microns. The scaffold consists of two main components, nanofibers and intermittent plain surfaces (Fig. 1B). The latter were designed to provide mechanical support to the fibers during the lithography and as an internal control to compare axonal growth in presence of aligned nanofibers or a 2D plain surface of IP-Dip polymer (Fig. 1B). In order to allow for cell culture, we designed Polydimethylsiloxane (PDMS) rings to be applied on the glass substrate where the scaffolds are printed (Fig. S1A–C). We fabricated the rings by printing 3D molds, which were then used for pouring and curing the PDMS in the desired shape (Fig. S1A–B). The final chambers were then assembled by fixing the PDMS rings on glass slides with the 3D scaffold (Fig. S1C).

We characterized the surface of the fibers using scanning electron microscopy (SEM). SEM images documented the successful scaffold printing (Fig. 1B). Fiber diameter and inter-fiber spacing were confirmed as 1 μm and 5 μm respectively (Fig. 1Bi & Bii). The surface of the fibers displayed two longitudinal grooves, which provide a larger surface area for more efficient cell adhesion and can act as guides for directional axonal growth (Fig. 1Bii). Further, porosity analysis of the nanogrid structure was performed by optical microscopy and SEM. Indeed, light microscopy analysis showed light passing through the pores of the grid (Fig. S1D). SEM analysis confirmed the area of the pores to be 25 μm² (Fig. 1B).
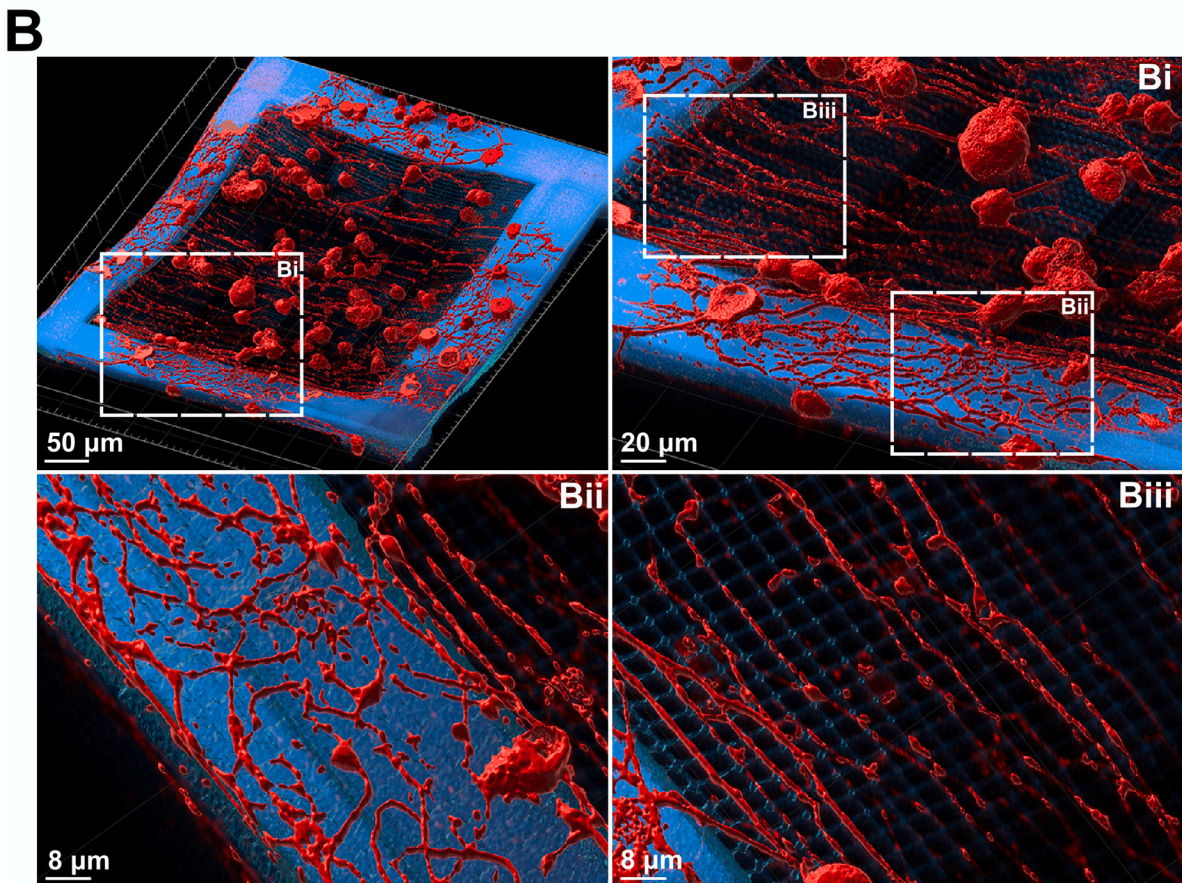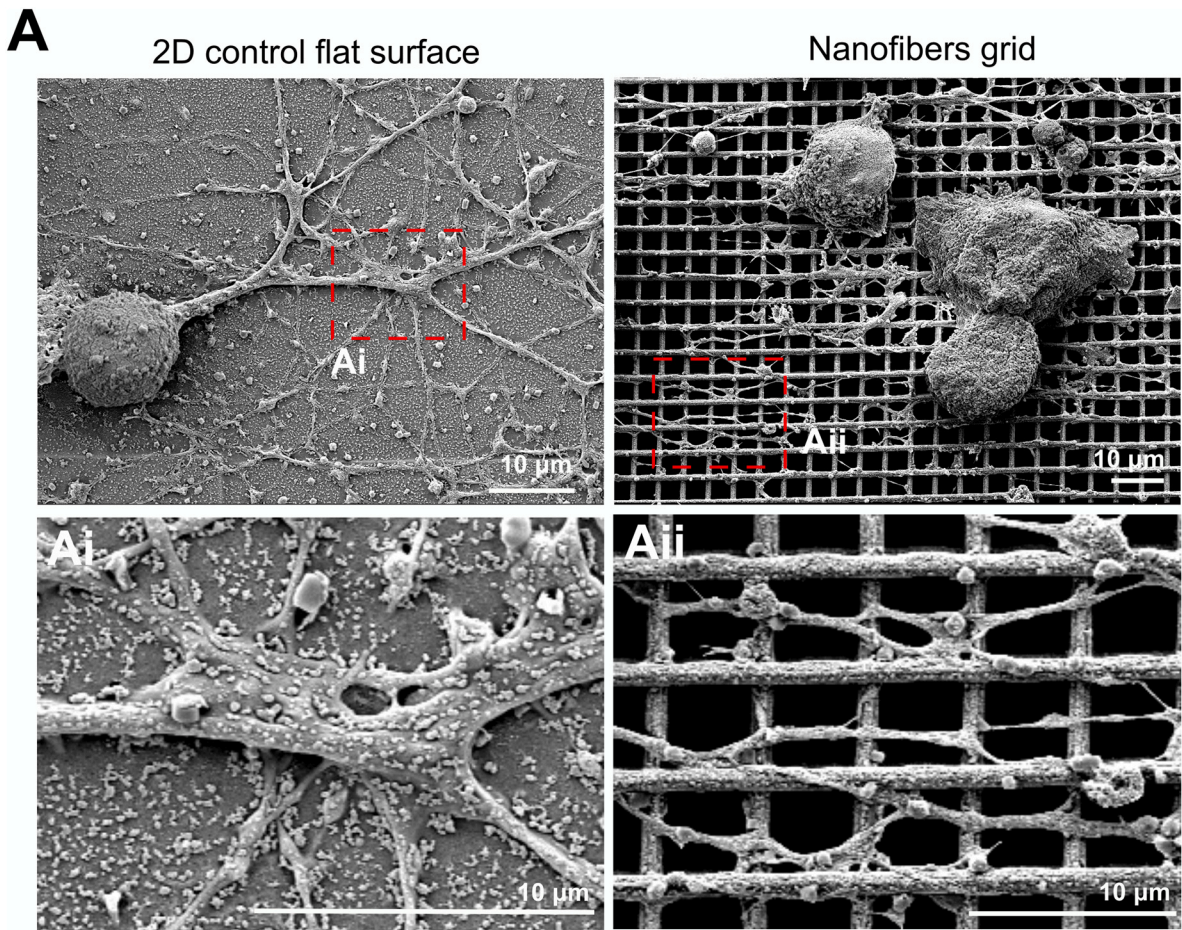
Fig. 3. DRG neurons can be cultured on IP-Dip fibers. (A) SEM images of DRG neurons growing on the 2D control surface and fibers of the IP-Dip scaffold. Magnified views are shown of the branching axonal growth on glass (Ai), *vs* the nerve bundles observed on the fibers (Aii). (B) 3D surface rendering of DRG neurons growing on top and on the side of the IP-Dip scaffold from confocal images where the neurons were stained with anti-βIII-tubulin antibody (in red). Intrinsic auto-fluorescence of the IP-Dip polymer observed with 405 nm excitation wavelength has been used to better visualize the scaffold (in blue). Bird's eye (Bi) and magnified views highlighting the radial growth of axons on 2D IP-Dip surface(Bii) and the vectorial growth on the aligned fibers of the nanogrid (Biii). Scale bars: 100 μm (A), 50 μm (B), 20 μm (Bi), 8 μm (Bii & Biii). (For interpretation of the references to color in this figure legend, the reader is referred to the web version of this article.)

3.2. Physio-chemical characterization

We investigated the physical and chemical properties of photo-lithographed IP-Dip structures, by determining their thermal and mechanical features as well as their hydrophilicity (see Table 1). Thermal and mechanical stability are essential parameters for biomaterials to maintain a particular structure over a period of time. We determined the thermal properties of our 3D IP-Dip scaffolds by differential scanning caliometry (DSC; Fig. 2A). The samples were heated from 40 °C to 250 °C at a rate of 10 °C/min and then cooled back to 40 °C at a rate 10 °C/min. During the heating cycle, we observed a peak consistent with a melting temperature (T_m,) of 220.06 ± 2.441 °C (Fig. 2A). We did not detect a peak during the cooling cycle, suggesting that no crystallization of the polymer occurred (Fig. 2A). The calculated T_m suggests that photolithographed IP-Dip structures are thermally stable. IP-Dip photolithographed 3D scaffolds are, thus, suitable candidates to be used as an implant or conduit *in vivo*.

To measure the mechanical strength of our scaffolds, we used nanoindentation atomic force microscopy (AFM) to generate maps of Young's modulus distribution concurrently with topographical imaging to map the anisotropic distribution of mechanical strength (Fig. 2B). As expected, the value of the Young's modulus varied in accordance with the structure of the fiber (Fig. 2Bi & ii), with the center of the fiber having a higher value than its periphery (Fig. 2Bii). The calculated mean value of Young's modulus for the 3D scaffold is 594.35 ± 73.01 MPa, indicating a considerable potential for the photolithographed nanofibers to sustain their spatial architecture and mechanical properties and suggesting their suitability as implant material for a variety of tissues, ranging from CNS or soft tissues to bone and cartilage.

We also analyzed the emission properties of photolithographed IP-Dip scaffolds. IP-Dip was highly fluorescent when excited with a laser at a wavelength of 405 and 488 nm (Fig. S2A & C), while the fluorescence of the material was significantly less pronounced when subjected to excitation using a wavelength of 568 nm (Fig. S2B & C).

The wettability of IP-Dip surfaces is an important parameter to determine their suitability as a biological support. The contact angle is a quantitative measure of the wetting of a solid by a liquid and is dependent on the surface area, with higher surface energies being associated with lower contact angles [33]. Surfaces which display angles lower than 90° are considered hydrophilic. Though the observed mean value of the contact angle for IP-Dip surfaces (77.702 ± 5.580°, Fig. 2C) is higher than that of traditional fused silica glass surface (37.53 ± 0.933°, Fig. 2C), it is still suggestive of the material hydrophilicity.

In summary, the measured thermal and mechanical features as well as the hydrophilicity of photolithographed IP-Dip structures are compatible with their use as a support for cellular growth in an *in vitro* and *in vivo* setting.

3.3. Quantification of cell viability and biocompatibility

Because of their relevance to peripheral injury, we tested the biocompatibility of IP-Dip scaffolds with adult mouse DRG neurons. Flat 3 mm × 3 mm × 10 μm (L × W × H) IP-Dip scaffolds were coated with poly-L-Lysine and laminin, two ECM proteins, which are critical for the successful attachment and growth of these neuronal types in culture.

Subsequently, neurons were seeded on the scaffold and allowed to grow for 48 h before being incubated with a commercially available fluorescent dye capable of labelling dead cells by reacting with intracellular amines (Fig. S3A & B). No significant difference in cell viability (Fig. 2D) or percentage of dead cells (Fig. S3C) was detected, suggesting that IP-Dip polymeric surfaces display similar level of biocompatibility for DRG neurons as traditional materials like fused silica glass.

We then tested our 3D nanofiber scaffold and allowed DRG neurons to grow on it for 48 h before being fixed and processed for SEM and confocal analysis. Again, successful growth of DRG neurons on IP-Dip fibers was confirmed by both SEM (Fig. 3A) and confocal imaging (Fig. 3B). No noticeable effects on neuronal viability or sign of axonal stress were observed when comparing nanofibers to the flat control IP-Dip surface (Fig. 3A & B). Visual inspection of DRG neurons neurite outgrowth on the 2D IP-Dip surface using SEM and fluorescence microscopy confirmed that axons extend radially in all possible angles (360°) from the soma as they would on glass (Fig. 3A, left panel; Fig. 3B). In contrast, axons running on IP-Dip fibers followed the funnels as predicted (Fig. 3A, right panel; Fig. 3B).

We also tested the biocompatibility of IP-Dip with an additional neuronal type, mouse motor neurons (MNs), which are central to peripheral and spinal cord injury. We derived MNs from mouse embryonic stem cells (mESCs) and cultured them on IP-Dip nanogrid scaffolds for 3–4 days (Fig. S4). SEM analysis confirmed successful attachment of the MNs to both the fibers and 2D surface of the scaffold (Fig. S4). Again, no issues regarding cell viability or axonal degeneration were visually detected. Thus, our data support the biocompatibility of IP-Dip and its suitability for a range of neuronal types.

3.4. Quantification of the directionality of axonal outgrowth

We confirm the vectorized axonal growth on the IP-Dip fibers by analyzing the local orientation distribution of axons on glass, 2D IP-Dip surface and IP-Dip fibers (Fig. 4A & B). Indeed, quantification of axonal orientation on glass resulted in a widely distributed local pixel orientation between 90° and −90°, indicating no directional specificity (Fig. 4B). Similarly, axonal preferential alignment towards 0°, 45°, and 90° was observed on 2D IP-Dip control surfaces (Fig. 4B). This slight shift towards particular angles might be due to the roughness of the grid surface in comparison with the smooth glass surface. On IP-Dip fibers, the printed longitudinal grooves played a crucial role in directing the growth of axons (Fig. 4A), as highlighted by the narrow distribution of local pixel orientation between 90° and −90°, (Fig. 4B, right most panel), indicating vectorized growth parallel to horizontal x-axis (0°).

We calculated the orientation index (OI) as described in the Methods section, and performed statistical analysis to determine the directional specificity of DRG axons. OI value (mean ± s.e.m.; in a.u.) of axons on IP-Dip fibers (0.28 ± 0.027) is approximately 5 times higher (**$p < 0.01$) than those on glass surface (0.048 ± 0.015) (Fig. 4C). Similarly, OI of axons on IP-Dip fibers is approximately 9 times higher (***$p < 0.001$) than those on 2D IP-Dip surface (0.029 ± 0.042) (Fig. 4C). No significant difference was observed between glass and 2D IP-Dip surface (Fig. 4C).

Further, normalized pixel frequency orientation was categorized in 6 clusters/bins (−90° to −60°, −60° to −30° and −30° to 0°, 0° to 30°, 30° to 60°, 60° to 90°) and plotted against the angular range of each bins
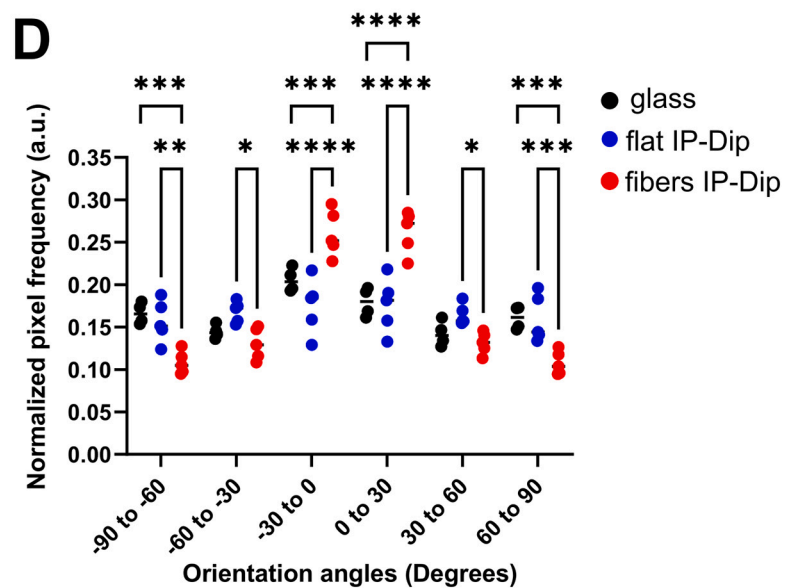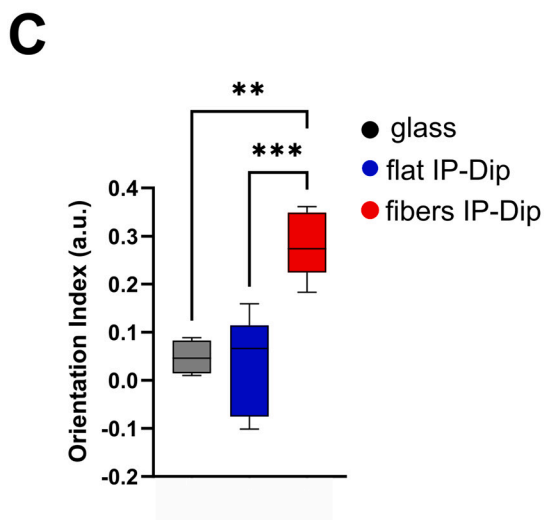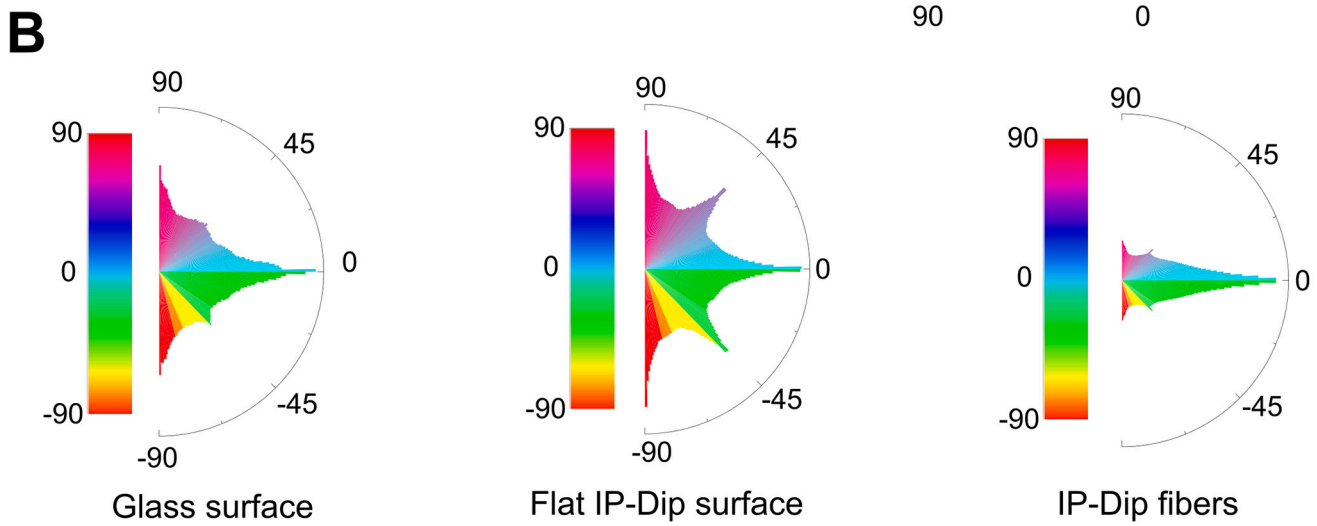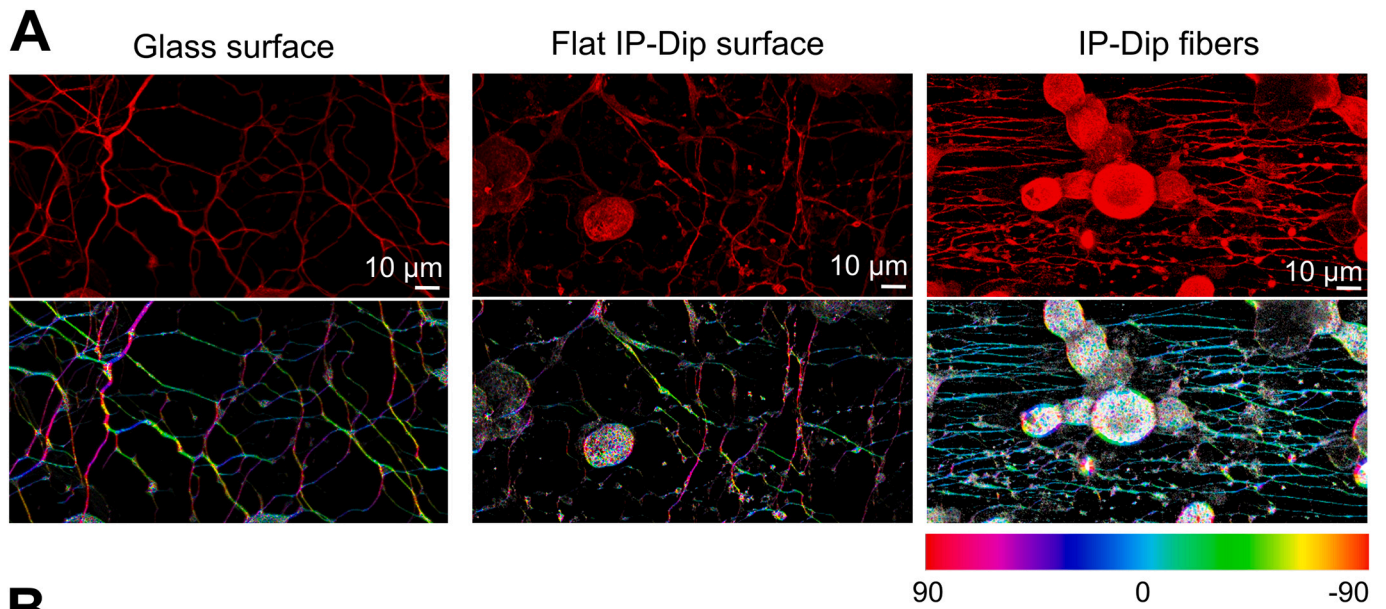
Fig. 4. Quantification of axons orientation on glass, 2D IP-Dip surface and IP-Dip fibers. (A) DRG neurons were grown on glass, 2D IP-Dip surface and IP-Dip fibers for 2 days before being fixed and stained for with anti-βIII-tubulin antibody (in red). Color-mapped imaged generated using the OrientationJ plugin of ImageJ as described in the Materials and Methods section are shown for each condition. Scale bar: 10 μm. (B) Normalized polar frequency histograms of axonal orientation angles from 3 independent experiments ($n = 3$) are also shown. (C) Plot of orientation index calculated from the angle orientation of DRG neuron axons on glass, 2D IP-Dip surface and IP-Dip fibers surface. (D) Plot of normalized pixel frequency of the axonal orientation binned in six categories ($-90°$ to $-60°$, $-60°$ to $-30°$, $-30°$ to $0°$, $0°$ to $30°$, $30°$ to $60°$ and $60°$ to $90°$) between $-90°$ to $90°$. Data are shown as mean $\pm$ s.e.m.; asterisks indicate statistical significance (One-way ANOVA with Tukey's *post hoc* test; *$p < 0.05$, **$p < 0.01$, ***$p < 0.001$, ****$p < 0.0001$). (For interpretation of the references to color in this figure legend, the reader is referred to the web version of this article.)

◄──────────────────

(Fig. 4D). Most pixels of neurons cultured on IP-Dip fibers were in the angular range of $-30°$ to $30°$ contrary to glass (****$p < 0.0001$) and 2D IP-Dip surface (****p < 0.001).

3.5. Orchestrated neuronal 3D growth inside IP-Dip scaffolds

We tested a variation of our 3D scaffold design to evaluate how different geometries and layer interspacing could promote DRG neurons penetration into the IP-Dip structure. We designed a 1mm × 0.5mm × 0.1 mm (L × W × H) nanogrid with 1 μm fibers and an anisotropic inter-fiber spacing ranging from 25 to 50 μm (Fig. 5A). This orchestrated 3D scaffold with predominantly unidirectional orientation of parallel microfibrils harbouring nanogrooves has been reported to be ideal for the culture of eukaryotic cells [31]. The space in-between layers is comparable to the size of DRG neuron somata (around 30 μm) to facilitate their even distribution throughout the different layers of the scaffold.

Indeed, we found that, unlike our previous design, DRG neurons were able to populate the entirety of the scaffold (Fig. 5B & D). Cells were detected on each layer of the aligned fibers and axonal growth was not restricted to the individual layers of aligned fibers, with axons crossing layers and creating a true 3D network (Fig. 5B & D). Interestingly, axons were able to follow the orientation of the fibers in individual layers from the place of attachment up to the length of the fiber (1 mm), creating a parallel orchestrated network of axons in each layer (Fig. 5C). For these reasons, this modified design proved itself to be superior to our original one by retaining its ability to promote vectorized growth of axons on a layer to layer basis, while also allowing for the penetration of cells inside the structure and the establishment of an orchestrated 3D axonal network. These features are very promising for future *in vivo* applications, where the design could serve as a general template, with modification of parameters such as number of layers, interfiber orientation and spacing to accommodate for different needs, lesion types and tissue or cell types.

4. Discussion

Effective therapeutic strategies for severe PNI and SCI are still limited [12,38], and include the use of implants to stabilize the spinal cord [13], auto grafting and systemic injection of growth factors [13]. Motor/sensory neuron loss of function, neuronal degeneration and mismatch of damaged nerve and graft dimensions are known drawbacks of these approaches. Meta-analysis of more than 70 preclinical studies suggests that combination of cell therapy with various scaffolds improves function restoration when compared to cell therapy alone [39,40]. Several polymer-made scaffolds have been investigated, including gelatin, laminin, collagen, silicon, polyaniline (PANi), and poly-hydroxyl butyrate (PHB). Nonetheless it is still a major challenge to engineer an ideal nanofibrous scaffold that provides an attractive clinical alternative to nerve auto grafts and semiconductor implants for SCI [41,42], and severe technical limitations still exist for the development of free standing scaffold for 3D growth of cells [24]. Hydrogel materials, which are able to provide 3D micro environments, often lack fine control of their geometrical micro- and nano-scale features, crucial for guiding cell development and alignment of inter-cellular connections [43]. The use of direct laser fabrication techniques allow for better control over the dimension and shape of 3D scaffolds [28,43]. Indeed, the use of 2-PP photolithography has been explored in the creation of patterns and

scaffolds at a micro-scale to facilitate the guided growth, proliferation, and differentiation of neurons [29,30]. These studies, however, did not account for cellular 3D growth [29,30]. We expanded upon the concepts presented in previous studies by designing orchestrated nanofibrous 3D scaffolds, with nano-scale features imprinted on the fibers, to direct the growth of axons. In addition, our multi-layered design allowed for 3D growth of neurons inside the scaffold (Fig. 5B), paving the way for the development of further constructs with the aim of facilitating the reconstruction of complex tissues. Thus, the current study provides a proof of concept that orchestrated nanofiber 3D scaffolds promote vectorized growth of axons along the length of nanofibers. Indeed, recent studies showed how aligned fibers enhanced stem cell attachment, migration, and differentiation *via* facilitating the increased expression of cytoskeletal proteins such as integrin, MMP1 and TIMP4 to improve the interaction of cells with scaffold matrix [44,45]. For the scaffold fabrication we used a synthetic polymer (IP-Dip resist), which allowed us to finely control our fiber's features. Indeed, SEM analysis confirmed successful printing of 200 nm wide longitudinal clefts on the fiber surface (Fig. 1Bii). Recently, increasing efforts have been directed towards the development of biodegradable photoresist, susceptible to enzymatic degradation, such as Trimethylsilyl cellulose (TMSC) based photoresist, which can be degraded using the endopeptidase enzyme Chymotrypsin, secreted by the exocrine pancreas [46,47]. IP-Dip is a poly-acryl formulation that can be degraded by the breakdown of the ester group cross-linking (patent application N[0] PCT/JP2016/051585) [48]. We further coated our scaffold (and the control glass surface) with poly-L-lysine and laminin to promote the attachment of neuronal cells to the rough surface of the fibers. Poly-L-lysine is a cationic polymer, which facilitates the attachment of cells, while laminin is a major functional component of basal lamina which surrounds the CNS and PNS during their development and control the expansion, migration and differentiation of neural stem cells (NSCs) [10]. Combinatorial effect of the fiber rough surface, longitudinal clefts and laminin coating increased the attachment and survival of neurons. We did not observe any difference in the number of viable neurons between control glass and IP-Dip surfaces (Fig. S3).

The adult DRG neurons used in this study are characterized by a single process that bifurcates into a peripheral and a central axonal branch, thus mainly displaying axonal projections, which simplify the observation of axonal growth patterns [49]. DRG neurons cultured on glass surface and 2D IP-Dip surface grew radially from the soma in any favorable direction. In contrast, axonal growth on IP-Dip fibers was directional (Fig. 4). Our results are in agreement with the recently published paper by Eunhee Kim et al. [26], where the authors used photolithographed magnetically actuated microbots to induce the vectorized growth of axons. Interestingly, the authors reported that while axons extended parallel to the x-axis (0°), they did not do so in the orthogonal direction along the fibers oriented in the y-axis (90°). Similarly, we designed the fibers so that the continuity of the fibers in the orthogonal direction (y-axis) is hindered by the fibers in upper layer (horizontally aligned in x-axis), creating a mechanical constraint to prevent neurite orthogonal growth. This was done in preparation of the engineering of implants for use *in vivo*, where directing axonal growth along a main axis would be advantageous. Indeed, aligned fibers can promote the vectorized growth of residual axons at the site of injury and help repair the function of the damaged nerve tissue [50–52]. Previous studies reported that neuronal cells reprogram themselves after
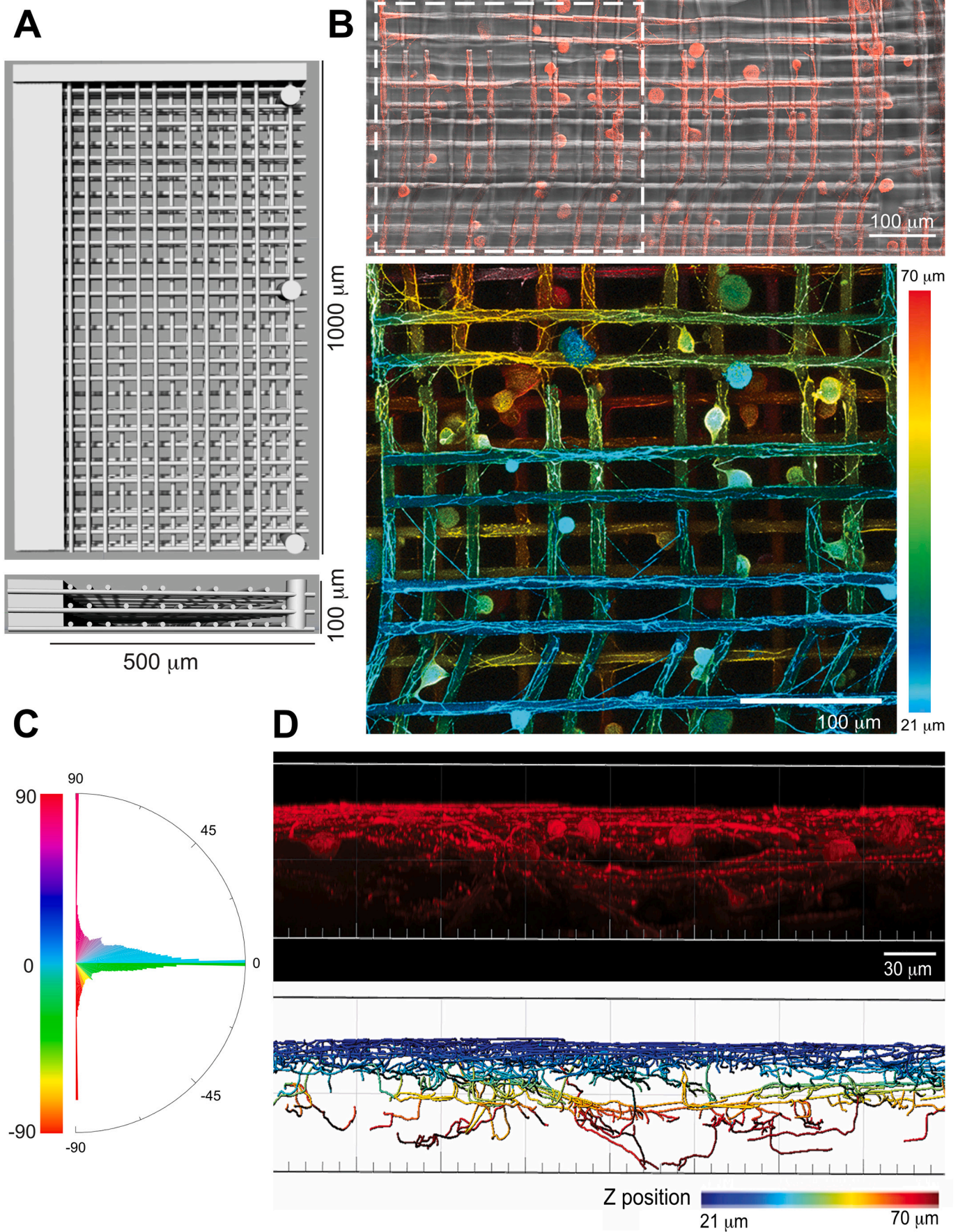
(caption on next page)

Fig. 5. 3D culture of DRG neurons inside an anisotropic IP-Dip scaffold. (A) 3D design of the anisotropic scaffold. The dimensions of the scaffold are as follows: 1000 μm long, 500 μm wide, and 100 μm thick with heterogeneous interfiber space (≥25 μm). The distance between different layers was kept at 30 μm. (B) Fluorescence image of βIII-tubulin stained DRG neurons (in red) grown in the scaffold. A magnified panel, color coded by the relative position in the Z-axis, is provided to better visualize the 3D growth of axons and neurons inside the structure. Scale bar 100 μm. (C) Polar frequency histogram of pixel orientation showing the angular range of the axons from 90° to −90°. (D) Maximum projection on the Z-axis of DRG neurons growing in the 3D IP-Dip scaffold stained for βIII-tubulin (in red). The panel underneath is a 3D surface rendering of the axons from the maximum projection above, which better illustrates the axonal network in 3D. Axons are color coded according with their position on the Z-axis. Scale bar 30 μm. (For interpretation of the references to color in this figure legend, the reader is referred to the web version of this article.)

neuronal damage to grow directionally for axon reconnection with their targets [53,54]. We also experimented with a re-designed scaffold devoid of the aforementioned mechanical constraints and with an inner layer spacing optimized for the penetration of DRG neurons cell bodies (Fig. 5A). Interestingly, while neurons could grow inside the scaffold and project axons in 3D, bridging between different fiber layers, axonal growth was still vectorized along the fibers within each individual layer (Fig. 5B–D). Thus, in our study, we have successfully cultured mESC derived motor neurons (Fig. S4) and DRG neurons on 3D IP-Dip scaffolds (Figs. 3–5 & S3) and showed that axons are extending in a direction-specific manner. Taken together with previous work, our study highlights a possible use for aligned scaffold/conduits/implants to promote the vectorized growth of axons to repair the damaged nerve tissue at the site of injury.

5. Conclusions

The current *ex vivo* study demonstrates that highly aligned nanofibrous 3D scaffolds can efficiently promote an orchestrated 3D growth of neurons and a vectorized growth of axons along the length of the nanofibers. Our results suggest that DRG axons follow the length of fibers when cultured on our nanogrid, while lacking specific alignments on glass and 2D IP-Dip surfaces. This observation was compounded by calculating an orientation index for neurons cultured on aligned nanogrid fibers, glass and 2D IP-Dip surfaces. Thus, photolithographed aligned scaffold/conduits/implants alone or combined with neural stem cells could be used to facilitate reconnection and repair of the damaged nerves after the injury. Further, *in vivo* analyses will be required to explore clinical applications of this technology.

Supplementary data to this article can be found online at https://doi.org/10.1016/j.msec.2021.112502.

CRediT authorship contribution statement

LA and MT conceived the project and performed the experiments reported in the study. MS provided support and guidance for the printing of 3D scaffolds through the use of 2-PP laser lithography. LG acquired and processed confocal images from the scaffolds. LA analyzed the data. LA and MT wrote the manuscript. MS and LG participated to the editing of the manuscript. LA, LG and MT prepared the figures.

Funding

Availability of the data and materials

We have provided all the data required for the publication. All the data presented in this manuscript are freely available upon request.

Informed consent

All authors have read the final draft and approved for the submission to the journal.

Ethical approval

N/A.

Human rights

N/A.

Declaration of competing interest

The authors declared no potential conflicts of interest with respect to the research, authorship, and/or publication of this article.

Acknowledgments

References

[1] Y. Kang, H. Ding, H. Zhou, et al., Epidemiology of worldwide spinal cord injury: a literature review, JN 6 (2017) 1–9.

[2] Repair, protection and regeneration of peripheral nerve injury, Neural Regen. Res. 10 (2015) 1777–1798.

[3] Richard McMurtrey, Novel advancements in three-dimensional neural tissue engineering and regenerative medicine, Neural Regen. Res. 10 (2015) 352–354.

[4] N. Rajabzadeh, E. Fathi, R. Farahzadi, Stem cell-based regenerative medicine, Stem Cell Investig. (2019) 6, https://doi.org/10.21037/sci.2019.06.04. Epub ahead of print 18 July.

[5] H. Cao, T. Liu, S.Y. Chew, The application of nanofibrous scaffolds in neural tissue engineering, Adv. Drug Deliv. Rev. 61 (2009) 1055–1064.

[6] S.K. Vimal, N. Ahamad, D.S. Katti, A simple method for fabrication of electrospun fibers with controlled degree of alignment having potential for nerve regeneration applications, Mater. Sci. Eng. C Mater. Biol. Appl. 63 (2016) 616–627.

[7] M. Zhu, W. Li, X. Dong, et al., In vivo engineered extracellular matrix scaffolds with instructive niches for oriented tissue regeneration, Nat. Commun. 10 (2019) 4620.

[8] C.S. Barros, S.J. Franco, U. Müller, Extracellular matrix: functions in the nervous system, Cold Spring Harb. Perspect. Biol. 3 (2011), a005108.

[9] J. Xue, T. Wu, Y. Xia, Perspective: aligned arrays of electrospun nanofibers for directing cell migration, APL Mater. 6 (2018), https://doi.org/10.1063/1.5058083. Epub ahead of print December.

[10] T.L. Jenkins, D. Little, Synthetic scaffolds for musculoskeletal tissue engineering: cellular responses to fiber parameters, NPJ Regen. Med. 4 (2019) 15.

[11] D.S. Kohane, R. Langer, Polymeric biomaterials in tissue engineering, Pediatr. Res. 63 (2008) 487–491.

[12] G. Hussain, J. Wang, A. Rasul, et al., Current status of therapeutic approaches against peripheral nerve injuries: a detailed story from injury to recovery, Int. J. Biol. Sci. 16 (2020) 116–134.

[13] P. Jendelova, Therapeutic strategies for spinal cord injury, Int. J. Mol. Sci. (2018) 19, https://doi.org/10.3390/ijms19103200. Epub ahead of print 18 July.

[14] M.F.B. Daud, K.C. Pawar, F. Claeyssens, et al., An aligned 3D neuronal-glial co-culture model for peripheral nerve studies, Biomaterials 33 (2012) 5901–5913.

[15] J.I. Kim, T.I. Hwang, L.E. Aguilar, et al., A controlled Design of Aligned and Random Nanofibers for 3D bi-functionalized nerve conduits fabricated via a novel electrospinning set-up, Sci. Rep. 6 (2016) 23761.

[16] A. Subramanian, U.M. Krishnan, S. Sethuraman, Fabrication of uniaxially aligned 3D electrospun scaffolds for neural regeneration, Biomed. Mater. 6 (2011), 025004.

[17] T. Wu, D. Li, Y. Wang, et al., Laminin-coated nerve guidance conduits based on poly(l-lactide-co-glycolide) fibers and yarns for promoting schwann cells' proliferation and migration, J. Mater. Chem. B 5 (2017) 3186–3194.

[18] J. Xue, D. Pisignano, Y. Xia, Maneuvering the migration and differentiation of stem cells with electrospun nanofibers, Adv. Sci. (Weinheim, Ger.) 7 (2020) 2000735.

[19] N.W. Garrigues, D. Little, C.J. O'Conor, et al., Use of an insulating mask for controlling anisotropy in multilayer electrospun scaffolds for tissue engineering, J. Mater. Chem. 20 (2010) 8962–8968.

[20] S.A. Sell, M.J. McClure, C.E. Ayres, et al., Preliminary investigation of airgap electrospun silk-fibroin-based structures for ligament analogue engineering, J. Biomater. Sci. Polym. Ed. 22 (2011) 1253–1273.

[21] F. Yang, R. Murugan, S. Wang, et al., Electrospinning of nano/micro scale poly(L-lactic acid) aligned fibers and their potential in neural tissue engineering, Biomaterials 26 (2005) 2603–2610.

[22] W. Zhou, Z. Li, Q. Zhang, et al., Gas flow-assisted alignment of super long electrospun nanofibers, J. Nanosci. Nanotechnol. 7 (2007) 2667–2673.

[23] D. Li, L. Tao, Y. Shen, et al., Fabrication of multilayered nanofiber scaffolds with a highly aligned nanofiber yarn for anisotropic tissue regeneration, ACS Omega 5 (2020) 24340–24350.

[24] R. Ng, R. Zang, K. Yang, Three-dimensional fibrous scaffolds with microstructures and nanotextures for tissue engineering, RSC Adv. 2 (2012) 10110–10124.

[25] S. Wu, Y. Wang, P.N. Streubel, et al., Living nanofiber yarn-based woven biotextiles for tendon tissue engineering using cell tri-culture and mechanical stimulation, Acta Biomater. 62 (2017) 102–115.

[26] E. Kim, S. Jeon, H.-K. An, A magnetically actuated microrobot for targeted neural cell delivery and selective connection of neural networks, Sci. Adv. (2020) 6, https://doi.org/10.1126/sciadv.abb5696. Epub ahead of print September.

[27] M. Hippler, E.D. Lemma, S. Bertels, et al., 3D scaffolds to study basic cell biology, Adv. Mater. 31 (2019) 1808110.

[28] F. Sala, C. Ficorella, R. Martínez Vázquez, et al., Rapid prototyping of 3D biochips for cell motility studies using two-photon polymerization, Front. Bioeng. Biotechnol. 9 (2021) 289.

[29] A. Marino, G. Ciofani, C. Filippeschi, et al., Two-photon polymerization of sub-micrometric patterned surfaces: investigation of cell-substrate interactions and improved differentiation of neuron-like cells, ACS Appl. Mater. Interfaces 5 (2013) 13012–13021.

[30] C. Fendler, C. Denker, J. Harberts, et al., Microscaffolds by direct laser writing for neurite guidance leading to tailor-made neuronal networks, Adv. Biosyst. 3 (2019) 1800329.

[31] V.P. Baklaushev, V.G. Bogush, V.A. Kalsin, et al., Tissue engineered neural constructs composed of neural precursor cells, recombinant spidroin and PRP for neural tissue regeneration, Sci. Rep. 9 (2019) 3161.

[32] Lagaly, G.B.V. Derjaguin, N.V. Churaev, V.M. Müller, Surface forces, Consultants Bureau, New York, London 1987, Ber. Bunsenges. Phys. Chem. 92 (1988) 1058.

[33] P. Morouço, S. Biscaia, T. Viana, et al., Fabrication of poly(ε-caprolactone) scaffolds reinforced with cellulose nanofibers, with and without the addition of hydroxyapatite nanoparticles, Biomed. Res. Int. 2016 (2016) 1596157.

[34] K. Ben-Yaakov, S.Y. Dagan, Y. Segal-Ruder, et al., Axonal transcription factors signal retrogradely in lesioned peripheral nerve, EMBO J. 31 (2012) 1350–1363.

[35] M. Terenzio, M. Golding, G. Schiavo, siRNA screen of ES cell-derived motor neurons identifies novel regulators of tetanus toxin and neurotrophin receptor trafficking, Front. Cell. Neurosci. 8 (2014) 140.

[36] M. Hafezparast, R. Klocke, C. Ruhrberg, et al., Mutations in dynein link motor neuron degeneration to defects in retrograde transport, Science 300 (2003) 808–812.

[37] L. Agrawal, S.K. Vimal, T. Shiga, Role of serotonin 4 receptor in the growth of hippocampal neurons during the embryonic development in mice, Neuropharmacology 158 (2019), 107712.

[38] A.F. Cristante, T.E.P.de Barros Filho, R.M. Marcon, Therapeutic approaches for spinal cord injury, Clinics (Sao Paulo) 67 (2012) 1219–1224.

[39] N. Romanyuk, T. Amemori, K. Turnovcova, et al., Beneficial effect of human induced pluripotent stem cell-derived neural precursors in spinal cord injury repair, Cell Transplant. 24 (2015) 1781–1797.

[40] V.P. Baklaushev, V.G. Bogush, V.A. Kalsin, et al., Tissue engineered neural constructs composed of neural precursor cells, recombinant spidroin and PRP for neural tissue regeneration, Sci. Rep. 9 (2019) 3161.

[41] H. Amani, H. Kazerooni, H. Hassanpoor, et al., Tailoring synthetic polymeric biomaterials towards nerve tissue engineering: a review, Artif. CellsNanomed. Biotechnol. 47 (2019) 3524–3539.

[42] R. Boni, A. Ali, A. Shavandi, et al., Current and novel polymeric biomaterials for neural tissue engineering, J. Biomed. Sci. 25 (2018) 90.

[43] A. Accardo, M.-C. Blatché, R. Courson, et al., Direct laser fabrication of free-standing PEGDA-hydrogel scaffolds for neuronal cell growth: engineering 3D biocompatible microenvironments, Mater. Today 21 (2018) 315–316.

[44] E. Schnell, K. Klinkhammer, S. Balzer, et al., Guidance of glial cell migration and axonal growth on electrospun nanofibers of poly-epsilon-caprolactone and a collagen/poly-epsilon-caprolactone blend, Biomaterials 28 (2007) 3012–3025.

[45] S. Wang, S. Zhong, C.T. Lim, et al., Effects of fiber alignment on stem cells-fibrous scaffold interactions, J. Mater. Chem. B 3 (2015) 3358–3366.

[46] D. Gräfe, M. Gernhardt, J. Ren, et al., Enzyme-degradable 3D multi-material microstructures, Adv. Funct. Mater. 31 (2021) 2006998.

[47] A. Wolfberger, A. Petritz, A. Fian, et al., Photolithographic patterning of cellulose: a versatile dual-tone photoresist for advanced applications, Cellulose (Lond) 22 (2015) 717–727.

[48] D.J. Carbaugh, S. Kaya, F. Rahman, Transparent and visible light-insensitive acrylic photoresist for negative tone optical lithography, J. Vac. Sci. Technol. B 35 (2016), 011601.

[49] A. Ribeiro, S. Vargo, E.M. Powell, et al., Substrate three-dimensionality induces elemental morphological transformation of sensory neurons on a physiologic timescale, Tissue Eng. A 18 (2011) 93–102.

[50] M.H. Tuszynski, O. Steward, Concepts and methods for the study of axonal regeneration in the CNS, Neuron 74 (2012) 777–791.

[51] T.A. Hadlock, C.A. Sundback, D.A. Hunter, A polymer foam conduit seeded with Schwann cells promotes guided peripheral nerve regeneration, Tissue Eng. (2000), https://doi.org/10.1089/107632700320748. Epub ahead of print 008.

[52] A.R. Filous, J.M. Schwab, Determinants of axon growth, plasticity, and regeneration in the context of spinal cord injury, Am. J. Pathol. 188 (2018) 53–62.

[53] K.R. Jessen, P. Arthur-Farraj, Repair schwann cell update: adaptive reprogramming, EMT, and stemness in regenerating nerves, Glia 67 (2019) 421–437.

[54] Y. Zhang, W. Li, T. Laurent, et al., Small molecules, big roles – the chemical manipulation of stem cell fate and somatic cell reprogramming, J. Cell Sci. 125 (2012) 5609–5620.